Ionics (2012) 18:781–786
DOI 10.1007/s11581-012-0747-3

SHORT COMMUNICATION

Preparation of PtSnRh/C-Sb_2O_5·SnO_2 electrocatalysts by an alcohol reduction process for direct ethanol fuel cell

J. C. Castro · R. M. Antoniassi · R. R. Dias · M. Linardi · E. V. Spinacé · A. Oliveira Neto

Received: 17 February 2012 / Revised: 26 April 2012 / Accepted: 17 May 2012 / Published online: 1 June 2012

Abstract PtSnRh/C-Sb_2O_5·SnO_2 electrocatalysts with different Pt/Sn/Rh atomic ratios (90:05:05, 70:25:05, and 50:45:05) were prepared by an alcohol reduction process using H_2PtCl_6·$6H_2O$, $SnCl_2$·$2H_2O$, $RhCl_3$·xH_2O as metal sources, ethylene glycol as solvent and reducing agent, and a physical mixture of Vulcan XC72 (85 wt%) and Sb_2O_5·SnO_2 (15 wt%) as support. The electrocatalysts were characterized by X-ray diffraction and transmission electron microscopy. The electro-oxidation of ethanol was studied by cyclic voltammetry and chronoamperometry at 25 and 50 °C and in single direct ethanol fuel cell (DEFC) at 100 °C. The diffractograms of PtSnRh/C-Sb_2O_5·SnO_2 electrocatalysts showed the peaks characteristic of Pt face-centered cubic structure and several others peaks associated with ·SnO_2 and Sb_2O_5·SnO_2. Transmission electron micrographs of PtSnRh/C-Sb_2O_5·SnO_2 electrocatalysts showed the metal nanoparticles distributed on the supports with particle sizes of about 2–3 nm. The electrochemical measurements and the experiments in a single DEFC showed that PtSnRh/C-Sb_2O_5·SnO_2 (90:05:05) and PtSnRh/C-Sb_2O_5·SnO_2 (70:25:05) electrocatalysts exhibited higher performance for ethanol oxidation in comparison with PtSnRh/C electrocatalyst.

Keywords PtSnRh/C-Sb_2O_5·SnO_2 · Alcohol reduction process · Ethanol electro-oxidation · Fuel cells

Introduction

The development of new electrocatalysts for the electro-oxidation of ethanol has received much attention, because the ethanol is produced in large quantities from biomass and is much less toxic than others alcohol and it also presents more convenient distribution logistics [1].

The platinum is commonly used as anode or cathode in direct alcohol fuel cell, even though the platinum alone is not a good electrocatalyst for the ethanol oxidation, consequently the addition of co catalysts to platinum is necessary [1–3].

PtSn have been considered the most active electrocatalysts for ethanol electro-oxidation. However, due to the difficulty of C–C bond breaking, the principal products formed are acetaldehyde and acetic acid; consequently, the addition of a third metallic element to PtSn could improve the performance of ethanol electro-oxidation in a single cell [1–3].

The addition of Rh to the PtSn/C electrocatalysts has been reported to increase CO_2 production and/or improve the performance of ethanol electro-oxidation in a single cell and direct ethanol fuel cell (DEFC) [4–9]. Antoline [8, 9] using cyclic voltammetry experiments showed that Pt–Sn–Rh (1:1:0.3 and 1:1:1) electrocatalysts synthesized by reduction of the metal precursors with formic acid were more effective for ethanol electro-oxidation than the binary Pt–Sn catalyst. Similar results were described by Spinacé [7] in a DEFC operating at 100 °C where PtSnRh/C (50:45:05) electrocatalyst was more active than PtSn/C (50:50) electrocatalyst. García-Rodríguez [1] described that the electro-oxidation of ethanol to CO_2 is only marginally promoted by the addition of Rh to PtSn/C; however, it was observed a higher production of acetic acid on the Rh-modified PtSn/C electrodes, which was responsible for the higher current density observed.

Another alternative to increase the performance of the electrocatalysts for ethanol electro-oxidation was the deposit of Pt, Sn, and Rh on the surface of metal oxides such as CeO_2, RuO_2, or SnO_2 [10–15]; however, these oxides have poor electron conductivity at low temperatures. Recently, it has been proposed that the use of Sb-doped SnO_2 (Sb_2O_5·SnO_2,

J. C. Castro · R. M. Antoniassi · R. R. Dias · M. Linardi · E. V. Spinacé · A. O. Neto (✉)
Instituto de Pesquisas Energéticas e Nucleares–IPEN-CNEN/SP,
Av. Prof. Lineu Prestes, 2242, Cidade Universitária,
05508-900 São Paulo, SP, Brazil
e-mail: aolivei@ipen.br

ATO) that has an enhancement of electrical conductivity compared to SnO_2, CeO_2, or others oxides [16, 17].

Oliveira Neto [16] showed that Pt nanoparticles supported on a physical mixture of carbon and ATO were more active for ethanol oxidation in acidic medium compared to Pt nanoparticles supported only on ATO or on carbon support. The enhancement of activity was attributed to better dispersion of Pt particles on the ATO support, as well as to the effects of SnO_2 adjacent to Pt (bifunctional effect and/or the electronic effect) [16, 17]. Ayoub [18] also showed that PtSn/C-Sb_2O_5·SnO_2 (50:50) electrocatalysts prepared by an alcohol-reduction process exhibited higher performance for ethanol oxidation in comparison with PtSn/C (50:50).

In this context, the aim of this work was prepare PtSnRh/C-Sb_2O_5·SnO_2 electrocatalysts with different Pt/Sn/Rh atomic ratios by an alcohol reduction process and to test these electrocatalysts for ethanol electro-oxidation. The obtained results were compared with PtSnRh/C (50:45:05) electrocatalyst prepared by alcohol reduction process, because it has been described as the most active ternary composition for the ethanol electro-oxidation [7].

Experimental

PtSnRh/C-Sb_2O_5·SnO_2 electrocatalysts (20 % of metal loading, with Pt/Sn/Rh ratio atomics of 90:05:05, 70:25:05, and 50:45:05) were prepared in a single step by an alcohol reduction process [6, 7] using H_2PtCl_6·$6H_2O$, $SnCl_2$·$2H_2O$, and $RhCl_3$·xH_2O as metal sources, ethylene glycol as solvent and reducing agent and a physical mixture of Vulcan XC72 (85 wt%) and Sb_2O_5·SnO_2 (15 wt%) as supports.

PtSnRh/C and PtSnRh/C-Sb_2O_5·SnO_2 electrocatalysts were characterized by X-ray diffraction (XRD) using a Rigaku diffractometer model Miniflex II using Cu Kα radiation source (l=0.15406 nm). The diffractograms were recorded in the range of 2θ=20–90° with a step size of 0.05° and a scan time of 2 s per step, while that the morphology, distribution, and size of the nanoparticles were observed with a JEOL transmission electron microscope (TEM) model JEM-2100 operated at 200 kV [7, 16]. Mean particle sizes were determined by counting more than 200 particles from different regions of each sample.

The cyclic voltammetry and chronoamperommetry measurements were carried out under controlled temperatures of 25 and 50±0.1 °C using a Nova Ética thermostat. These studies were performed using a Microquímica potenciostat, where the working electrodes (geometric area of 0.3 cm^2 with a depth of 0.3 mm) was prepared using the thin porous coating technique [7], the reference electrode was a reversible hydrogen electrode and the counter electrode was a Pt plate. The electrochemical measurements were realized in presence of 1.0 mol L^{-1} of ethanol +0.5 mol L^{-1} H_2SO_4 solutions saturated with N_2.

Direct ethanol fuel cell tests were performed using PtSnRh/C-Sb_2O_5·SnO_2 electrocatalysts as anode and Pt/C electrocatalysts as cathode in a single cell with an area of 5 cm^2. For direct ethanol fuel cell studies also, it was utilized the carbon–cloth teflon-treated as a gas diffusion layer and a Nafion® 117 membrane as electrolyte. The electrodes (anode or cathode) were hot pressed on both sides of a Nafion® 117 membrane at 100 °C for 2 min under a pressure of 225 kgf cm^{-2}. The electrodes prepared contained 1 mg Pt cm^{-2} in the anode and cathode. The temperature was set to 100 °C for the fuel cell and 80 °C for the oxygen humidifier, 2 mol L^{-1} ethanol aqueous solution was delivered at approximately 2 mL min^{-1} and the oxygen flow was set to 500 mL min^{-1} under 2 bar of pressure. The polarization curves were obtained using an electronic load [7].

Results and discussion

The X-ray diffractograms of PtSnRh/C (50:45:05), PtSnRh/C-Sb_2O_5·SnO_2 (90:05:05), PtSnRh/C-Sb_2O_5·SnO_2 (70:25:05), and PtSnRh/C-Sb_2O_5·SnO_2 (50:45:05) electrocatalysts are shown in Fig. 1. PtSnRh/C (50:45:05) showed a broad peak at about 25° that was associated with the Vulcan XC72 support material, four peaks at approximately 2θ=40°, 47°, 67°, and 82°, which are associated with the (111), (200), (220), and (311) planes, respectively, of the face-centered cubic (fcc) structure characteristic of platinum and platinum alloys and two peaks at approximately 2θ= 34° and 52° identified as a SnO_2 phase (cassiterite) [10]. For all PtSnRh/C-Sb_2O_5·SnO_2 electrocatalysts, besides the Pt (fcc) phase, it was also observed peaks at about 2θ=27°, 34°, 38°, 52°, 55°, 62°, 65°, and 66°, which were characteristic of cassiterite SnO_2 phase and SnO_2 and ATO used as

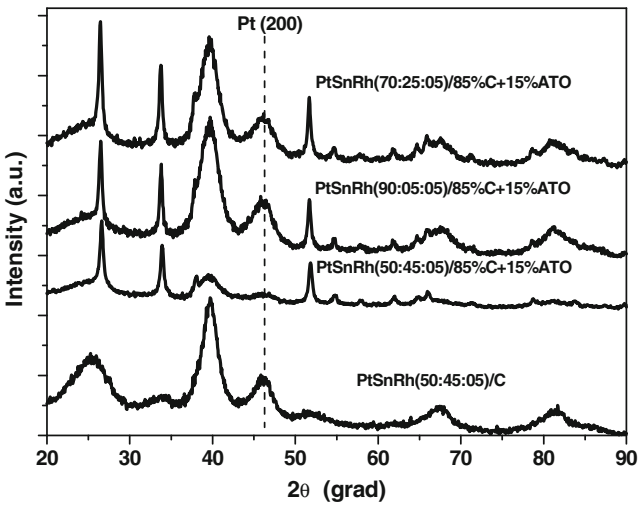

Fig. 1 X-ray diffractograms of the PtSnRh/C (50:45:05), PtSnRh/C-Sb_2O_5·SnO_2 (90:05:05), PtSnRh/C-Sb_2O_5·SnO_2 (70:25:05), and PtSnRh/C-Sb_2O_5·SnO_2 (50:45:05) electrocatalysts

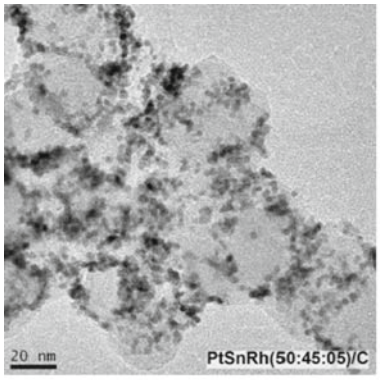

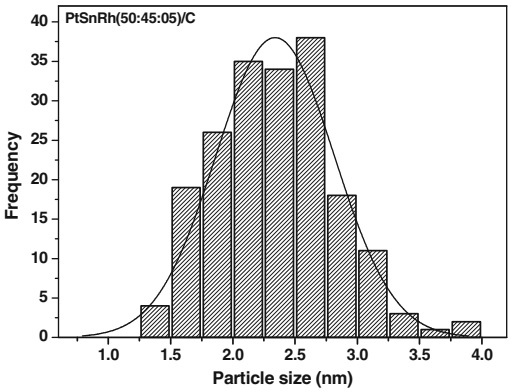

(a)

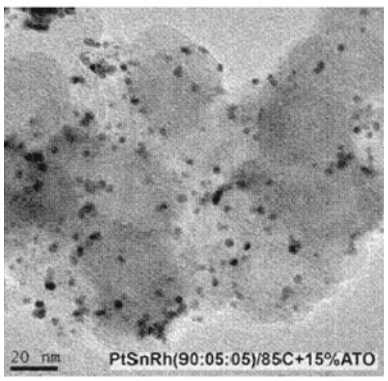

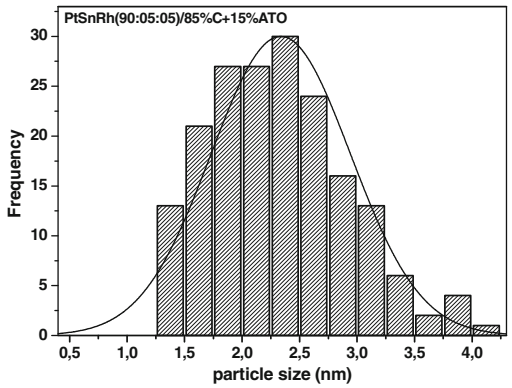

(b)

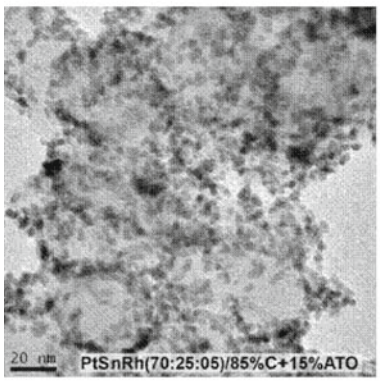

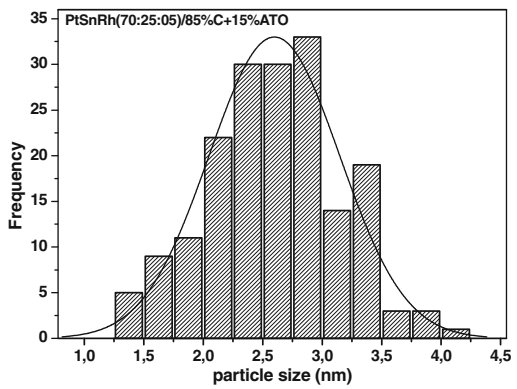

(c)

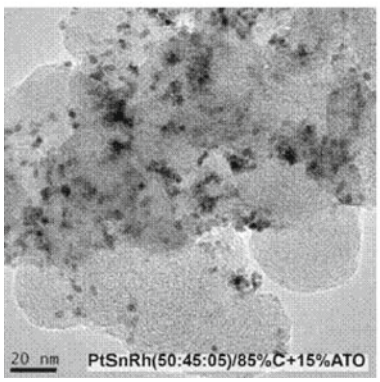

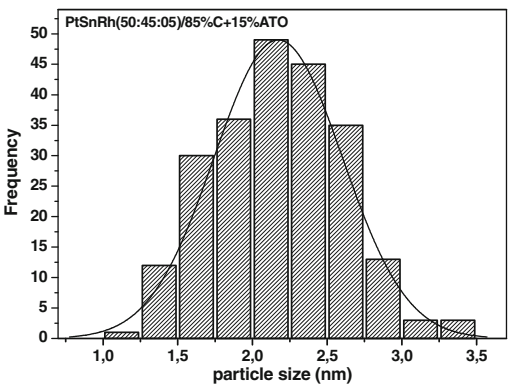

(d)

Fig. 2 TEM micrograph and a histogram of **a** PtSnRh/C (50:45:05), **b**PtSnRh/C-$Sb_2O_5{\cdot}SnO_2$ (90:05:05), **c** PtSnRh/C-$Sb_2O_5{\cdot}SnO_2$ (70:25:05), and **d** PtSnRh/C-$Sb_2O_5{\cdot}SnO_2$ (50:45:05) electrocatalyst with the mean diameter and particle distribution

support [16, 19]. The mean crystallite sizes were determined from the (200) plane of Pt (fcc) phase using Debye–Scherrer equation [20–22] and PtSnRh/C (50:45:05), PtSnRh/C-$Sb_2O_5{\cdot}SnO_2$ (90:05:05), PtSnRh/C-$Sb_2O_5{\cdot}SnO_2$ (70:25:05), PtSnRh/C-$Sb_2O_5{\cdot}SnO_2$ (50:45:05) electrocatalysts showed crystallite sizes of 3.0, 3.0, 2.9, and 2.5 nm, respectively.

Figure 2 presents TEM micrographs and a histogram with the mean particle size and particle distribution of the following electrocatalysts: PtSnRh/C (50:45:05)—Fig. 2a, PtSnRh/C-$Sb_2O_5{\cdot}SnO_2$ (90:05:05)—Fig. 2b, PtSnRh/C-$Sb_2O_5{\cdot}SnO_2$ (70:25:05)—Fig. 2c and PtSnRh/C-$Sb_2O_5{\cdot}SnO_2$ (50:45:05)—Fig. 2d, which showed average particle sizes of 2.3, 2.3, 2.6, and 2.2 nm, respectively. Thus, TEM results are in accordance with mean crystallite sizes calculated from XRD data. However, a good distribution of nanoparticles on the supports was observed only for PtSnRh/C-$Sb_2O_5{\cdot}SnO_2$ (90:05:05) while for other electrocatalysts some agglomerates were observed.

Figure 3 shows the cyclic voltammetry for ethanol oxidation using PtSnRh/C and PtSnRh/C-$Sb_2O_5{\cdot}SnO_2$ electrocatalysts at 25 °C (Fig. 3a) and 50 °C (Fig. 3b) in presence of 1.0 mol L^{-1} of ethanol and 0.5 mol L^{-1} of H_2SO_4. PtSnRh/C-$Sb_2O_5{\cdot}SnO_2$ (90:05:05) and PtSnRh/C-$Sb_2O_5{\cdot}SnO_2$ (70:25:05) electrocatalysts showed the highest current values at 25 and 50 °C in all potential range in comparison with PtSnRh/C-$Sb_2O_5{\cdot}SnO_2$ (50:45:05) and PtSnRh/C (50:45:05). For PtSnRh/C-$Sb_2O_5{\cdot}SnO_2$ (90:05:05) electrocatalyst the ethanol electro-oxidation started at approximately 0.20 and 0.15 V at the temperature of 25 and 50 °C, respectively.

Figure 4 shows the chronoamperometry curves for ethanol oxidation using PtSnRh/C (50:45:05), PtSnRh/C-$Sb_2O_5{\cdot}SnO_2$ (90:05:05), PtSnRh/C-$Sb_2O_5{\cdot}SnO_2$ (70:25:05) and PtSnRh/C-$Sb_2O_5{\cdot}SnO_2$ (50:45:05) electrocatalysts at 25 °C (Fig. 4a) and 50 °C (Fig. 4b) in the potential of 0.50 V for 30 min. Chronoamperometry results for ethanol electro-oxidation on PtSnRh/C and PtSnRh/C-$Sb_2O_5{\cdot}SnO_2$ at 25 °C showed a decay of current faster in the first 2 min followed by a slower decay. The final current values at 0.50 V (T=25 °C) increase in the following order: PtSnRh/C-$Sb_2O_5{\cdot}SnO_2$ (90:05:05)>PtSnRh/C-$Sb_2O_5{\cdot}SnO_2$ (70:25:05)>PtSnRh/C-$Sb_2O_5{\cdot}SnO_2$ (50:45:05)>PtSnRh/C (50:45:05), while at 50 °C the final current values increase in the following order: PtSnRh/C-$Sb_2O_5{\cdot}SnO_2$ (90:05:05)≈ PtSnRh/C-$Sb_2O_5{\cdot}SnO_2$ (70:25:05)>PtSnRh/C-$Sb_2O_5{\cdot}SnO_2$ (50:45:05)>PtSnRh/C (50:45:05). The current values obtained for PtSnRh/C-$Sb_2O_5{\cdot}SnO_2$ electrocatalysts were always higher than those obtained for PtSnRh/C in agreement with cyclic voltammetry experiments. The oxidation current density at 25 and 50 °C for all PtSnRh/C-$Sb_2O_5{\cdot}SnO_2$ electrocatalysts also decayed more slowly than that of the PtSnRh/C indicating the superior stability of these electrocatalysts. Similar results also

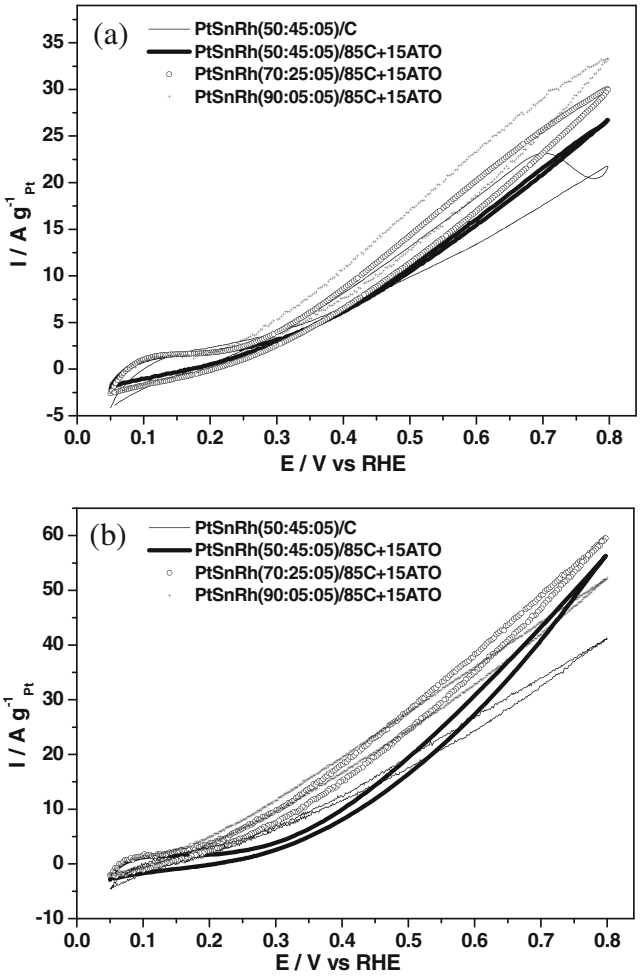

Fig. 3 Cyclic voltammograms of the PtSnRh/C (50:45:05), PtSnRh/C-$Sb_2O_5{\cdot}SnO_2$ (90:05:05), PtSnRh/C-$Sb_2O_5{\cdot}SnO_2$ (70:25:05), and PtSnRh/C-$Sb_2O_5{\cdot}SnO_2$ (50:45:05) electrocatalysts at 25 °C (**a**) and 50 °C (**b**) in 1 mol L^{-1} ethanol solution in 0.5 mol L^{-1} H_2SO_4 with a sweep rate of 10 mV s^{-1}

were observed by Oliveira Neto [23] for ethanol electro-oxidation using PtSn/CeO_2-C electrocatalyst. At 25 and 50 °C, it was also observed that the current values for ethanol electro-oxidation using PtSn/C-$Sb_2O_5{\cdot}SnO_2$ electrocatalysts decreased with the increase of Sn content. This behavior could be attributed to the fact that the electronic conductivity of tin oxide is poor and/or part of Pt active sites may be blocked by Sn [24].

Figure 5 show the performances of a single DEFC operating at 100 °C with PtSnRh/C (50:45:05), PtSnRh/C-$Sb_2O_5{\cdot}SnO_2$ (90:05:05), PtSnRh/C-$Sb_2O_5{\cdot}SnO_2$ (70:25:05), and PtSnRh/C-$Sb_2O_5{\cdot}SnO_2$ (50:45:05) as anode electrocatalysts. The results in DEFC are in good agreement with cyclic voltammetry and chronoamperometry experiments. The open circuit voltage of the fuel cell for PtSnRh/C-$Sb_2O_5{\cdot}SnO_2$ (70:25:05), PtSnRh/C-$Sb_2O_5{\cdot}SnO_2$ (90:05:05), PtSnRh/C-$Sb_2O_5{\cdot}SnO_2$ (50:45:05), and PtSnRh/C (50:45:05) electrocatalysts were 0.78, 0.75,

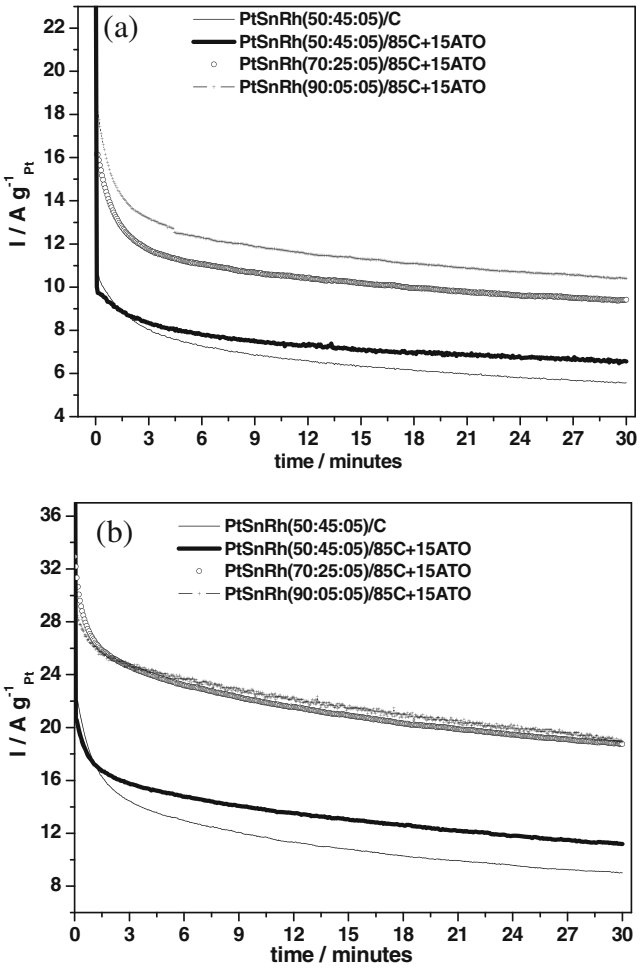

Fig. 4 Current–time curves at 0.50 V in 1 mol L^{-1} ethanol solution in 0.5 mol L^{-1} H_2SO_4 for PtSnRh/C (50:45:05), PtSnRh/C-Sb_2O_5·SnO_2 (90:05:05), PtSnRh/C-Sb_2O_5·SnO_2 (70:25:05) and PtSnRh/C-Sb_2O_5·SnO_2 (50:45:05) electrocatalysts at 25 °C (**a**) and 50 °C (**b**)

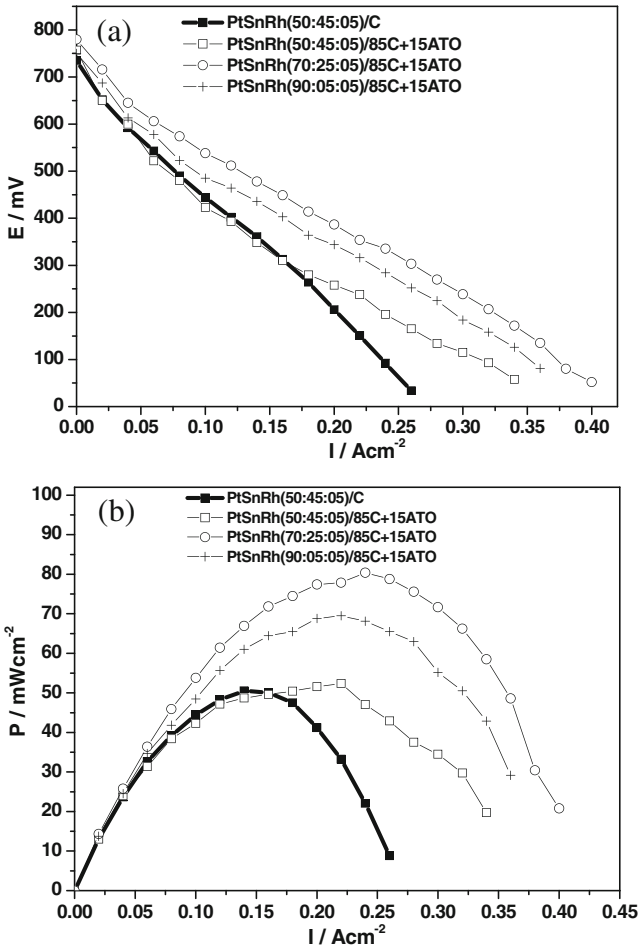

Fig. 5 I–V curves (**a**) and the power density (**b**) at 100 °C of a 5 cm^2 DEFC using PtSnRh/C (50:45:05), PtSnRh/C-Sb_2O_5·SnO_2 (90:05:05), PtSnRh/C-Sb_2O_5·SnO_2 (70:25:05) and PtSnRh/C-Sb_2O_5·SnO_2 (50:45:05) electrocatalysts

0.76, and 0.73 V, respectively. However, PtSnRh/C-Sb_2O_5·SnO_2 (70:25:05) electrocatalyst showed higher values of maximum power density (80 mW cm^{-2}) in comparison with PtSnRh/C-Sb_2O_5·SnO_2 (90:05:05; 70 mW cm^{-2}), PtSnRh/C-Sb_2O_5·SnO_2 (50:45:05; 53 mW cm^{-2}) and PtSnRh/C (50:45:05; 50 mW cm^{-2}). The experiments at 100 °C on single DEFC showed that the power density for the PtSnRh/C-Sb_2O_5·SnO_2 (70:25:05) electrocatalysts was 60 and 122 % higher than the ones obtained using PtSnRh/C (50:45:05) and PtSn/C (50:50) electrocatalysts [7], respectively.

The higher catalytic activity of PtSnRh/C-Sb_2O_5·SnO_2 electrocatalysts could be attributed to the synergy between the constituents of the electrocatalyst (metallic Pt and Rh, SnO_2 and Sb_2O_5·SnO_2), where SnO_2 or Sb_2O_5·SnO_2 strongly adsorbs water and precludes the Pt and Rh sites from reacting with H_2O to form M–OH, making Pt and Rh sites available for ethanol electro-oxidation [5, 6]. Thus, the presence of Sb_2O_5·SnO_2 could enhance the formation of chemisorbed oxygen species which promotes the oxidation of adsorbed carbon monoxide and/or intermediates species adsorbed on the surface of Pt and Rh sites. Also, Li [25] showed that carbon-supported Pt–Rh–SnO_2 electrocatalysts, consisting of PtRh alloy and a SnO_2 phase, have the capability in splitting C–C bond of ethanol molecule at room temperature and low potentials. The role of Rh was attributed to adsorb and stabilize the intermediate CH_2CH_2O, which leads to a cleavage of C–C bond at a reasonable speed. On the other hand, García-Rodríguez [1] studied the ethanol electro-oxidation using Rh-modified Pt_3Sn/C electrocatalyts and observed that the production of CO_2 was not greater on these catalysts as compared to Pt_3Sn/C. The higher activity of Rh-modified Pt_3Sn/C electrocatalyts was due the production of acetic acid and acetaldehyde. In this manner, the activity and selectivity of PtSnRh electrocatalysts for ethanol oxidation depends strongly on the catalyst preparation method which lead to different species present on the surface of the obtained materials.

Conclusions

The alcohol reduction process showed to be an effective method for producing in a single step of PtSnRh/C-$Sb_2O_5{\cdot}SnO_2$ for ethanol oxidation. The diffractograms of the PtSnRh/C-$Sb_2O_5{\cdot}SnO_2$ electrocatalysts showed the fcc structure of Pt and Pt alloys and several others peaks associated with SnO_2 and ATO used as support. Transmission electron micrographs for all electrocatalysts showed that the nanoparticles were distributed over the supports with average particle sizes in the range of 2–3 nm. The electrochemical measurements and the experiments in a single DEFC showed that PtSnRh/C-$Sb_2O_5{\cdot}SnO_2$ (90:05:05) and PtSnRh/C-$Sb_2O_5{\cdot}SnO_2$ (70:25:05) electrocatalysts exhibited higher performance for ethanol oxidation in comparison with PtSnRh/C electrocatalyst. Further work is now necessary to investigate the electrocatalyst surface by different techniques and to elucidate the mechanism of ethanol electrooxidation using these electrocatalysts.

Acknowledgments The authors thank the Laboratório de Microscopia do Centro de Ciências e Tecnologia de Materiais (CCTM) by TEM measurements, FAPESP (2011/18246-0), and CNPq (470790/2010-5) for the financial support.

References

1. García-Rodríguez S, Rojas S, Pena MA, Fierro JLG (2011) Appl Catal B Environ 106:520
2. Thole BT, Carra P, Sette F, Van der Laan G (1992) Phys Rev Lett 68:1943
3. Spinacé EV, Linardi M, Neto AO (2005) Electrochem Commun 7:365
4. De Souza JPI, Queiroz SL, Bergamaski K, Gonzalez ER, Nart FC (2002) J Phys Chem B 106:9825
5. Kowal A, Gojkovic SL, Lee KS, Olszewski P, Sung YE (2009) Electrochem Commun 11:724
6. Kowal A, Li M, Shao M, Sasaki K, Vukmirovic MB, Zhang J (2009) Nat Mater 8:325
7. Spinacé EV, Dias RR, Brandalise M, Linardi M, Neto AO (2010) Ionics 16:91
8. Antolini E (2007) J Power Sources 170:1
9. Colmati F, Antolini E, Gonzalez ER (2008) J Alloys Compd 456:264
10. Pan C, Li Y, Ma Y, Zhao X, Zhang Q (2011) J Power Sources 196:6228
11. Wu X, Scott K (2011) Int J Hydrogen Energy 36:5806
12. Piasentin RM, Spinace EV, Tusi MM, Neto AO (2011) Int J Electrochem Sci 6:2255
13. Liu H, Song C, Zhang L (2006) J Power Sources 155:95
14. Lux KW, Cairns EJ (2006) J Electrochem Soc 153:A1132
15. Delime F, Leger JM, Lamy C (1998) J Appl Electrochem 28:27
16. Neto AO, Brandalise M, Dias RR, Ayoub JMS, Silva AC, Penteado JC, Linardi M, Spinacé EV (2010) Int J Hydrogen Energy 35:9177
17. Lee KS, Park IS, Cho YH, Jung DS, Jung N (2008) J Catal 258:143
18. Ayoub JMS, Crisafulli R, Spinacé EV, Neto AO (2011) XVIII Sibee EC:246
19. Neto AO, Dias RR, Tusi MM, Linardi M, Spinacé EV (2007) J Power Sources 166:87
20. Sieben JM, Duarte MME (2011) Int J Hydrogen Energy 36:3313
21. Ayoub JMS, Geraldes AN, Tusi MM, Spinacé EV, Neto AO (2011) Ionics 17:559
22. Gupta SS, Singh S, Datta J (2009) Mater Chem Phys 116:223
23. Neto AO, Linardi M, dos Anjos DM, Tremiliosi G, Spinace EV (2009) J Appl Electrochem 39:1153
24. Li L, Huang M, Liu J, Guo Y (2011) J Power Sources 196:1090
25. Li M, Kowal A, Sasaki K, Marinkovi N, Su D, Korach E, Liu P, Adzic RR (2010) Electrochim Acta 55:4331